PALEOCEANOGRAPHY, VOL. ???, XXXX, DOI:10.1029/,

Mechanisms for millenial-scale global synchronization during the last glacial period

A. Timmermann,[1] U. Krebs,[2] F. Justino,[3] H. Goosse,[4] T. Ivanochko,[5]

Abstract. Global climate during the last glacial was punctuated by abrupt warmings and occasional pulses of freshwater into the North Atlantic that disrupted deep water production. These massive freshwater pulses known as Heinrich events arose in part, from instabilities within the Laurentide ice sheet. Paleo-evidence from the North Atlantic suggests that these events altered the production of deep water and changed downstream climate changes throughout the Northern hemisphere. In the tropical western Pacific sea surface temperatures and salinity varied together with ocean and climate changes at high latitudes. Here we present results from coupled modeling experiments that shed light on a possible dynamical link between the North Atlantic Ocean and the western tropical Pacific. This link involves a global oceanic standing wave pattern brought about by millennial-scale glacial density variations in the North Atlantic, atmospheric teleconnections triggered by meridional sea surface temperature gradients and local air-sea interactions. Furthermore, our modeling results are compared with hydrological records from the Cariaco basin, the Indian ocean, the Sulu Sea and Northern Australia.

1. Introduction

Proxy records covering Marine Isotope Stage 3 (MIS3, 60,000- 25,000 B.P.) reveal that the amplitude of climatic changes in the Northern Hemisphere during the last glacial period was greater than it has been during the Holocene. The last glacial period was characterized by (Dansgaard et al. [1993]) DO stadial-interstadial (cold-warm) transitions that involved abrupt temperature variations over Greenland of up to 16K (Lang et al. [1999], Severinghaus and Brook [1999]). In addition, this period was punctuated by Heinrich events that produced thick layers of ice rafted debris (IRD) in marine sediments throughout the North Atlantic (Heinrich [1988]). Heinrich events - massive surges of icebergs originating from the glacial ice sheets and shelves - were accompanied by cold conditions in the North Atlantic region, warm episodes in Antarctica (Blunier and Brook [2001]) and by increases of global sea level of up to 30 meters (Yokoyama et al. [2001], Sidall et al. [2003]). Furthermore, the associated millennial-scale North Atlantic density changes appear to have slowed or even terminated the meridional overturning circulation in the North Atlantic (Keigwin and Lehman [1994], Knutti et al. [2004]). While the amount of proxy-data documenting these transitions in the tropics is growing (e.g. Schultz and von Rad [1998], Peterson et al. [2000], Ivanochko et al. [2005], Turney et al. [2004]), the physical mechanisms responsible for these characteristic millennial-scale variations and their global teleconnections have not been fully disentangled.

Based on an intermediate tropical model, Cane [2002] argued that "abrupt" Northern Hemispheric transitions can be triggered remotely from abrupt orbitally-driven regime transitions of the El Niño-Southern Oscillation (ENSO). Evidence for tropical changes on millennial rather than precessional timescales, was recently provided by salinity reconstructions from the Pacific warm pool area (Stott et al. [2002]). It was shown (Stott et al. [2002]) that millennial-scale variations of the warm pool salinity varied with DO events in the North Atlantic (see Figure 1). Salinities decreased during interstadials and reversed during stadials (Stott et al. [2002])[1]. Because atmospheric teleconnections from the North Atlantic to the warm pool area were considered to be unlikely condidates to explain the observed correlation between the tropics and the Northern extratropics, Stott et al. [2002] suggested the millennial-scale variations in the North Atlantic were forced by ocean/atmospheric teleconnections analogous to the modern interannual variability associated with ENSO (Livezey et al. [1997]).

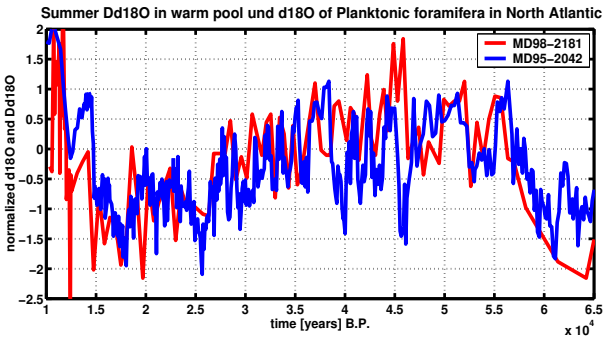

Figure 1. Extratropical-tropical connections: Normalized and inverted time series of Δ^{18}O of planktonic formanifera (red) in the Pacific warm pool core MD98-2181 (Stott et al. [2002]). The largest Δ^{18}O variations for Globigerinoides ruber represent local salinity variations and are coherent with the DO cycles, as recorded in the normalized δ^{18}O of planktonic foraminifera (blue) sampled off the Iberian margin (Shackleton et al. [2000]). Both records are shown on the GISP2 timescale (Blunier and Brook [2001]).

[1]International Pacific Research Center, University of Hawai'i, Honolulu, USA
[2]Leibniz Institut für Meereswissenschaften, IfM-GEOMAR, Kiel, Germany
[3]University of Toronto, Dept. of Physics, Toronto, ON Canada
[4]Université Catholique de Louvain, Institut d'Astronomie et de Géophysique, Louvain-la-Neuve, Belgium
[5]Department of Earth and Ocean Sciences, University of British Columbia, Vancouver, Canada

0883-8305/05/$12.00

As the changes in the North Atlantic and tropical Pacific occurred over millennia the term Super-ENSO was used to distinguish these changes from those associated with the modern interannual variability. In contrast to Stott et al. [2002] a recent analysis of a high-resolution record of surface moisture (Turney et al. [2004]) in Northern Australia suggests a link between an El Niño-like climate change pattern and interstadials in the North Atlantic, rather than a link between warm eastern-equatorial Pacific SST and stadial conditions in the North Atlantic. In both cases variations of salinity or precipitation have been connected to eastern equatorial temperature anomalies, rather than with oceanic changes and/or changes of the meridional position of the ITCZ. Our study presents evidence for a mechanism that can explain the link between tropical Pacific salinity and temperature and North Atlantic density anomalies triggered by either Heinrich or Dansgaard-Oeschger events. This mechanism involves pan-oceanic meridional changes in the position and strength of the Innertropical Convergence Zone (ITCZ) and baroclinic adjustments in the global ocean.

In section 2 we briefly describe the 5 modeling experiments conducted and analyzed here. Section 3 studies the atmospheric teleconnections of a shutdown of the meridional overturning circulation. Section 4 focuses on the oceanic component of the global teleconnection. The study concludes with a summary of our main results and a discussion thereof (section5).

2. Model experiments

The analysis is based on a series of global atmosphere-ocean-sea ice model simulations performed with the coupled model ECBilt-Clio. The atmospheric component ECBILT (Opsteegh et al. [1998]) of our coupled model is a 3-layer model with a quasi-geostrophic adiabatic core (Marshall and Molteni [1993]) and a set of physical parameterizations for the hydrological cycle (Held and Suarez [1978]) and a partly linearized radiation code. It runs in T21 triangular truncation, which corresponds to an approximate resolution of 5.6 in both latitude and longitude. The coupled ocean–sea ice model CLIO (Goosse et al. [1999]) is based on the primitive equations using a free surface and thermodynamic/dynamic assumptions, respectively. A parameterization of vertical mixing (Goosse and Fichefet [1999]) is used that represents a simplification of the Mellor and Yamada [1982] 2.5-level turbulence closure scheme. Furthermore, the ocean model CLIO includes mixing along isopycnals and it captures the effect of meso-scale eddies on transport (Gent and McWilliams [1990]). Furthermore, a paramterization for the dense water flow down topographic features (Campin and Goosse [1999]) is employed. The horizontal resolution of CLIO is 3 degrees, and there are 20 unevenly spaced vertical levels in the ocean. The individual models are coupled by exchanging momentum, freshwater, and heat. The simulations are performed with weak freshwater-flux corrections, which mostly affect the North Atlantic region. The model is freely available from http://www.knmi.nl/onderzk/CKO/ecbilt.html. In the standard model setup an inbalance in the global, interanual freshwater budget is compensated globally for numerical reasons. However, in our expeiment the inbalance associated with surging icebergs is intended and thus not compensated.

A 2000-year-long control simulation (**CTR**) represents pre-industrial climate with an atmospheric CO2 concentration of 0.28%. (Timmermann et al. [2004]). Figure 2, right panel

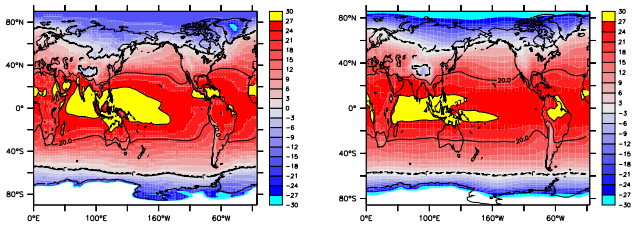

Figure 2. Left: Averaged ERA40 2m temperature, representing an estimate of the observed temperatures. Right: Simulated averaged 2m temperature for a 280 ppm CTR simulation using ECBilt-Clio.

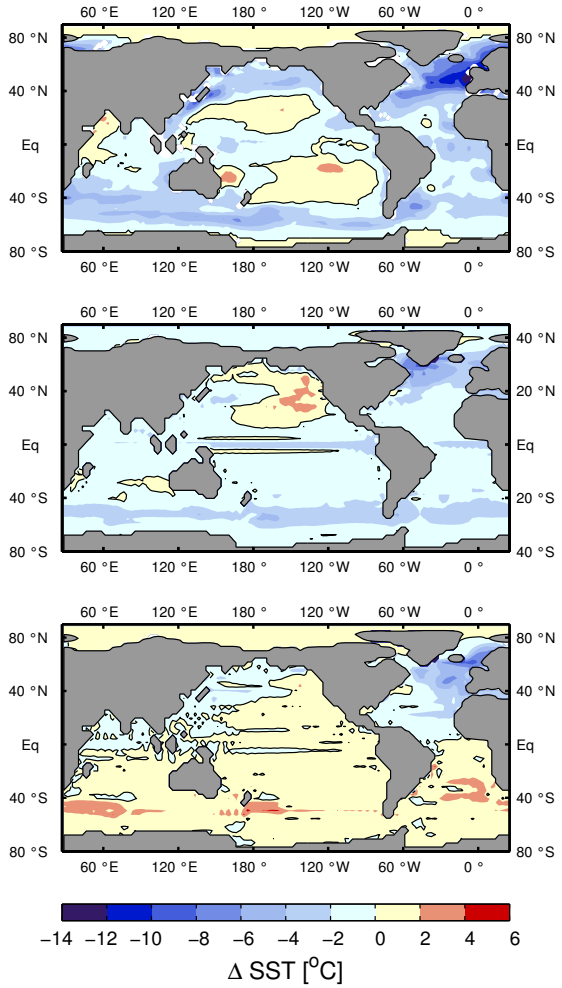

Figure 3. Reconstructed and simulated glacial sea surface temperature (SST) anomalies: Upper panel: Difference between reconstructed North Atlantic GLAMAP (Sarnthein et al. [2003]) and Pacific and Indian ocean (CLIMAP [1981]) sea surface temperature (time average of February and August) for the Last Glacial Maximum and the present-day SST (CLIMAP [1981]). Middle panel: Sensitivity of the simulated annual mean SST to glacial boundary conditions as quantified by the difference of the equilibrated time-mean SST of the LGM experiment and the pre-industrial CTR experiment. Lower panel: Simulated SST difference between a collapsed THC state during the LGM (time average of years 200-300 in experiment MW) and normal LGM conditions.

shows the simulated 2m air-temperature for pre-industrial conditions. It compares quite well with the ERA40 simulated 2m temperatures (Figure 2, left panel), although small differences in the CO_2 base state have to be considered.

The Last Glacial Maximum (**LGM**) simulation (Timmermann et al. [2004]) performed here utilizes the Peltier [1994] ice sheet topography of about 21,000 years ago, an ice sheet-albedo mask, reduced CO2 concentrations (200 ppm), modified orbital forcing, and a LGM vegetation index (Crowley and Baum [1997]) for which the deforested soils and plant cover are replaced by their respective glacial albedo. The inclusion of the ice sheet increases the albedo by more than 60% in North America and Europe. The associated changes in the river run-off and sea-level drop have not been included here. The surface climate of the 2000-year long LGM simulation equilibrates after about 500 years. The simulated North Atlantic sea surface temperature (SST) differences between LGM and CTR (Figure 3) are smaller than in recent SST reconstructions (Sarnthein et al. [2003]). Simulated LGM tropical sea surface temperature anomalies attain minimal values of -2K to -3K, consistent with alkenone reconstructions of (Lyle et al. [1992],Bard [2001]) and the cold tongue record of (Lea et al. [2000]). However, our modeling results exhibit a cold bias in the tropical Pacific compared to the CLIMAP reconstruction (CLIMAP [1981]) and the Galapagos record (Koutavas et al. [2002]) and a warm bias with respect to Hostetler and Mix [1999]. The simulated positive SST anomaly in the Northern Pacific (Figure 3) can be attributed to an overall weakening of the atmospheric westerlies in the North Pacific (Timmermann et al. [2004]). It bears some similarities with the CLIMAP reconstruction and a recent LGM modeling result (Kitoh et al. [2001]).

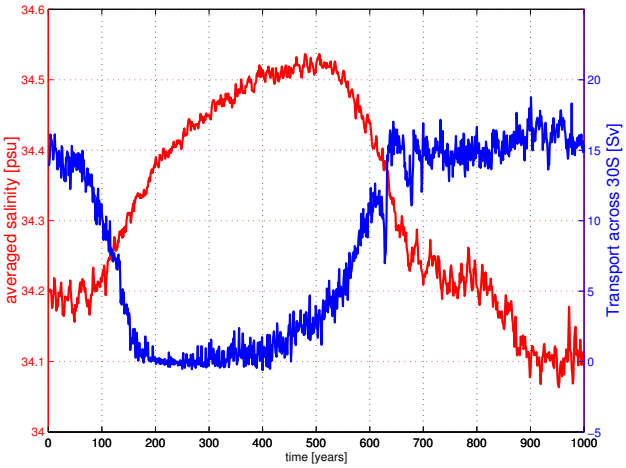

Figure 4. North Atlantic-tropical Pacific teleconnections: Simulated time series of the meridional ocean transport across 30S in the North Atlantic [Sv=10^6 x m^3/s] (blue) and area averaged salinity [psu] in the Pacific warm pool (15^{o}S-15^{o}N, 120^{o}E -160^{o}E) area.

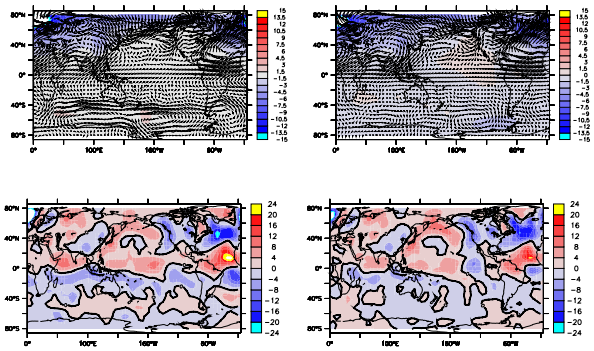

Figure 5. Atmospheric response to Heinrich event: Upper panels: Difference of time averaged wind stress (vectors), temperature (shading) fields of MW and LGM (left) and MW and MW2 (right). The time average is representing the THC shutdown state and is computed form the simulation years 250–300. Lower panels: Same as upper panels but for evaporation minus precipitation [cm/year].

At the core of our analysis is a transient meltwater (**MW**) experiment, which mimics the response of the glacial climate to a North Atlantic density perturbation, such as the one caused for instance by the Heinrich Event 2. A Gaussian-shaped (halfwidth 100 years) freshwater anomaly of 1.2 m/year (maximum value) is injected homogenously into the North Atlantic between 40^0-60^0N. This length is consistent with the most recent model-based estimates of Roche [2004]. The equivalent global sea-level rise of this hydrological forcing amounts to about 8m.

In order to study the atmospheric teleconnections more in detail two other meltwater experiments have been conduced. In **MW1** the atmosphere does not respond to SST anomalies triggered by the THC shutdown anywhere. In this sense the atmosphere is generating variability and air-sea fluxes based on global LGM SST climatology obtained from the LGM experiment. The atmosphere is decoupled from the actual ocean anomaly state in the globally, and the ocean is driven by simulated atmospheric heat-, freshwater, and momentum fluxes. The experiment **MW2** is very similar to MW1, with the main difference that the atmosphere in MW2 is insensitive to North Atlantic SST anomalies induced by the shutdown of the meridional overturning circulation, whereas it responds to SST anomalies elsewhere.

The physical mechanisms that generate DO events have not been disentangled yet. Some recent modeling evidence (Knutti et al. [2004]) suggests that DO events are associated with millennial-scale density-driven switches of the meridional overturning circulation in the North Atlantic. The origin of the initial density changes has not been identified unambiguously. They may be generated by internal oceanic processes (Timmermann et al. [2003]) or due to external forcing (Rahmstorf [2003]). Further changes of the sea-ice extend may help to amplify oceanic changes into relevant atmospheric changes. Hence, we submit that the diagnosed link between North Atlantic density anomalies and climate conditions in the Indian and Pacific oceans holds for stadial-interstadial transitions both with and without the involvement of Heinrich events.

The transient glacial meltwater pulse experiment (MW) leads to a complete shutdown of the North Atlantic meridional overturning circulation (see Figure 5), a cooling of the North Atlantic by about 6-8 K (Figure 3), and a complete recovery about 200 years after the anomalous freshwater forcing has been decreased to zero. The shutdown of the THC is accompanied by an increase in Pacific warm pool salinity (See Figure 5) of about 0.3-0.5 psu. This is less than the reconstructed local millennial-scale glacial salinity changes in the Sulu Sea. Furthermore, the MW experiment simulates a bipolar seesaw response (Figure 3), similar to the reconstructed North-South temperature gradient during Heinrich events (Stocker and Johnsen [2003],Knutti et al. [2004],).

3. Atmospheric teleconnections

In order to quantify the effect of the cold North Atlantic during the shutdown phase of the meridional overturning

circulation on the global atmospheric circulation we compute the anomalies of air temperature, wind-stress and evaporation minus precipitation as simulated by the MW simulation with respect to the LGM experiment as well as the anomalies simulated by the MW experiment with respect to the experiment MW2. The results (Figure 4) reveal that North Atlantic SST anomalies as depicted in Figure 3 influence the global climate. The downstream response of the North Atlantic cooling is a cooling over large parts of Asia, resulting in an enhanced meridional temperature contrast and hence a weaking of the annual mean winds over India and Southeast Asia and in particular of the summer monsoon circulation. This pronounced wind change is also reflected in an overall increase of evaporation minus precipitation in the Arabian Sea and Bay of Bengal and hence, drier conditions. This result is consistent with most recent reconstructions (Ivanochko et al. [2005]) of dustiness of Arabia, rainfall over India and the monsoon strength, as shown in Figure 6. In addition, we observe enhanced rainfall over evaporation in a band south of the equator in agreement with recent moisture reconstructions from Northern Australia (Turney et al. [2004]). Furthermore, as a result of cooling north and warming south of the equator our model simulates enhanced dryness and enhanced trade winds over northern South America. In the trade wind region also a positive air-sea feedback exists between SST, wind strength and evaporation. This model result is consistent also with the hydrological reconstructions of Peterson et al. [2000]. The tropical Atlantic atmospheric response to the dipole-like SST anomaly near the equator is reminiscent of a first order baroclinic response as predicted by the Gill [1980] theory. Evaporation minus precipitation changes of 5-10 cm/year can be found in the warm pool area which contributing to the increase of warm pool salinity during the THC shutdown phase (Figure 5). The freshwater flux anomalies in the warm pool may originate from the relatively weak Southern Indian warming (see Figure 3) during the Heinrich event. A dynamical linkage between an anomalously dry warm pool and positive Indian ocean SST anomalies during the Winter and Spring season has been proposed by Watanabe and Jin [2003] and Annamalei [2005], who argue that an Indian ocean warming triggers an atmospheric response in accordance with linear baroclinic first mode theory (Gill [1980]), which leads to a divergence in the warm pool area and hence to reduced precipitation. The atmospheric model employed here is capable of simulating such a kind of atmospheric response (Timmermann et al. [2004]) although its amplitude may be too weak, due to the quasi-geostrophic approximation and the low horizontal resolution of the model.

MW2 is designed such that the atmosphere is insensitive to North Atlantic SST anomalies induced by the shutdown of the THC. The left and right panels of Figure 4 – showing the effect only of North Atlantic SST anomalies – are very similar, except for smaller amplitudes in the tropics, simulated by MW2. This suggests that the main anomalous features of the atmospheric circulation discussed here directly result from the North Atlantic temperature anomalies and their downstream signature, in contrast to the assumptions of Stott et al. [2002]. This includes not only the changes of the monsoon circulations over Asia and South America but also an overall intensification of the trade winds in the Northern Hemispheric tropical Pacific. This will result in changes of the thermocline depth in the equatorial Pacific as will be discussed further below.

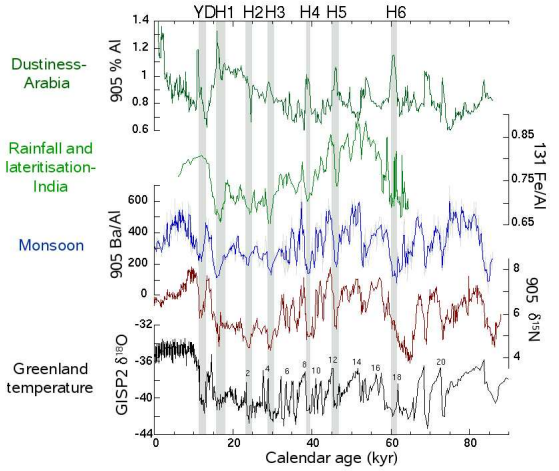

Figure 6. FIGURE for Tara From top to bottom: Arabian dustiness record ??; Lateralization; Productivity; GISP 2 $\delta^{18}O$.

These results illustrate the importance of the atmospheric bridge and local air-sea interactions to spread the signal from the Atlantic into the other ocean basins, supporting the conclusions of Dong and Sutton [2002].

4. Oceanic teleconnections

Density changes in the North Atlantic, as simulated by the glacial meltwater experiment (MW), lead to a global readjustment of the thermohaline circulation. This readjustment is established by the propagation of coastally and equatorially trapped Kelvin waves (Kawase [1987], Hsieh and Bryan [1996], Huang et al. [2000], Cessi et al. [2004], Johnson and Marshall [2002]). In coarse-resolution ocean models these waves, which establish the overall mass balance, are represented by viscous boundary waves (Hsieh et al. [1983]). Their characteristics depend partially on the numerical schemes employed by the ocean model and differ somewhat from those of free Kelvin waves. However, on long timescales such as those considered here this sensitivity can be disregarded. In the present simulation these waves propagate from the North Atlantic to the equator, they are forced to travel along the equator towards the coast of Africa, where they split into a northern and southern branch. While moving poleward, they radiate Rossby waves, which readjust the interior transport of the North and South Atlantic and weaken the boundary wave amplitude. The southern wave branch travels around the southern tip of South Africa into the Indian and subsequently the Pacific Ocean. The global baroclinic adjustment to an initial North Atlantic density anomaly takes from a few years to decades (Cessi et al. [2004]).

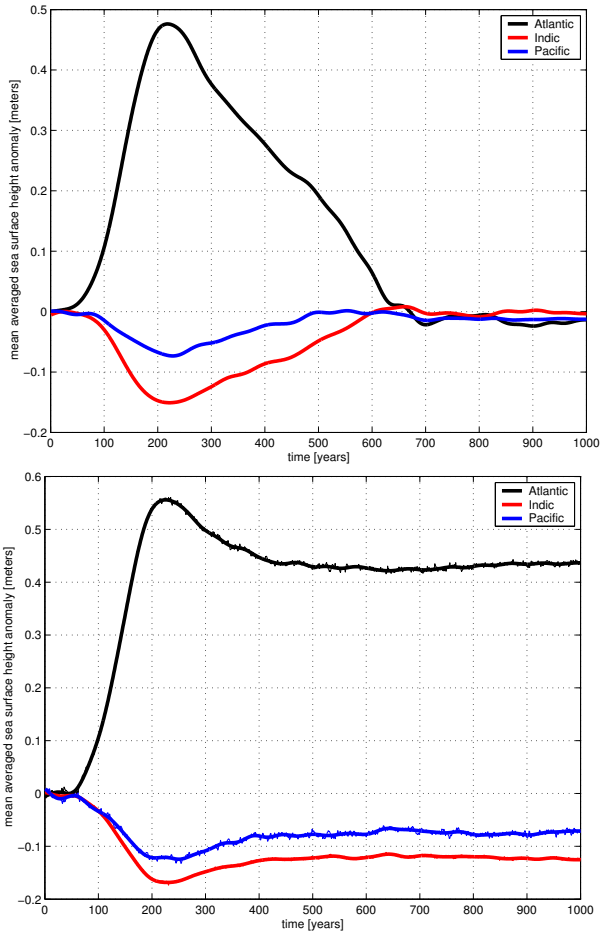

Figure 7. Global sea-level seiching: Left: Basin averaged sea level evolution [m] of the Atlantic, Pacific and Indian ocean basins simulated by the fully coupled meltwater experiment (MW). The sea level anomalies between Atlantic and Pacific exhibit an out-of-phase relationship which is typical for standing waves - so called global sea level seiches. Right: As left but for the global uncoupled experiment (MW1).

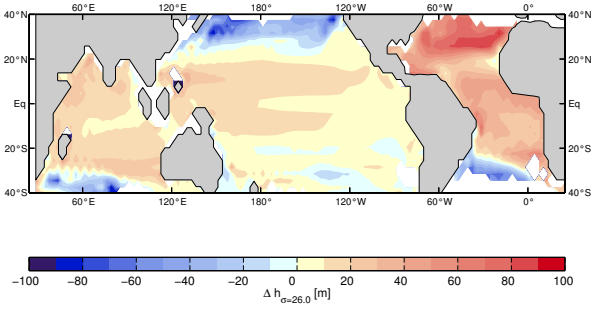

Figure 8. Thermocline response to a THC shutdown: Difference of the time-averaged depth of the isopycnal 26.0 kg/m^3 surface between a collapsed THC state (years 200-300 in MW) and an un-collapsed LGM THC state (years 1-30 in MW). The 26.0 kg/m^3 isopycnal surface separates upper-ocean thermocline waters from deep ocean waters. An overall deepening of the North Atlantic thermocline is accompanied by a deepening of the thermocline in the other tropical oceans.

The overall sea level and thermocline depth changes can be described in terms of a standing wave pattern (Figure 7) - a global seiche (Cessi et al. [2004]). In agreement with Cessi et al. [2004], a centennial sea level rise of about 40 cm in the North Atlantic is accompanied by an almost instantanous sea level drop of 15 and 8 cm in the Indian and Pacific ocean, respectively. The globally averaged sea-level signal has been removed from our analysis. Figure 7 reveals that the THC does not recover from its forced collapse for the MW1 experiment. However, during the initial shutdown stages (years 0-150), the dynamical behaviour resembles that of the MW experiment. Experiment MW1 highlights not only the importance of air-sea coupling for the recovery of the THC but also the importance of oceanic wave processes in establishing large-scale pan-oceanic connections on centennial to millennial timescales.

As predicted by simple shallow water models (Huang et al. [2000]) these global baroclinic readjustment processes are associated with thermocline changes in the Atlantic, the Indian and the Indian oceans. Figure 8 shows that a collapse of the meridional overturning circulation in the North Atlantic leads to changes in the depth of isopycnals characterizing thermocline waters in the tropical Indian and Pacific oceans by up to 20m, which is comparable to warm pool thermocline depth anomalies typically obtained during present-day ENSO events. However, it should be noted here that the simulated thermocline anomalies in Figure 8 originate from two sources: one is the oceanic global adjustment to North Atlantic density anomalies triggering Kelvin and Rossby waves and deepening the tropical Pacific thermocline. The other source is the equatorial trade wind intensification depicted in Figure 4 which is a direct result of hemispheric anomalies of the hemispheric temperature gradient during the Heinrich event. In case the thermocline signal has an SST manifestation, local positive air-sea interactions are expected to further modify the thermocline signal. It should also be noted that the Bjerknes positive air-sea feedback in the tropical Pacific is underestimated in our coupled model. Western tropical Pacific thermocline depth anomalies in the uncoupled simulation (MW1) attain values of 5-10m, as compared to simulated 20m in the fully coupled MW experiment and the MW2 simulation which disregards SST anomalies in the North Atlantic.

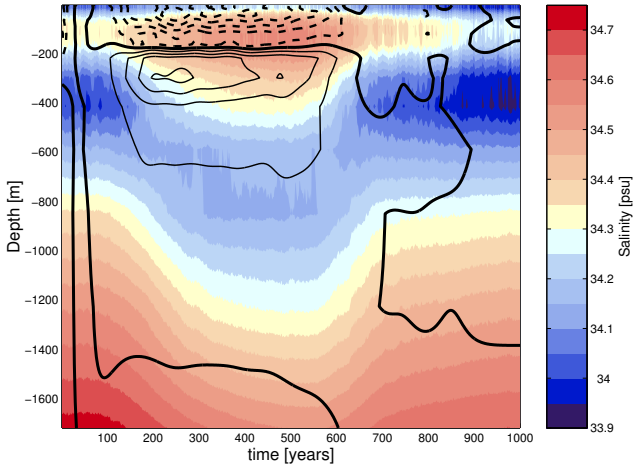

Figure 9. Mechanism for warm pool salinity changes: time-depth diagram of area-averaged salinity [psu] near the core site of MD98-2181 (shaded) and zonal currents (contour, the contour interval is 2 cm/s).

Locally the centennial-scale density and thermocline depth anomalies in the tropical Pacific are accompanied by currents anomalies. In MW the thermocline gradients as well as the intensification of the equatorial trade winds lead to a strengthening of the South Equatorial Current as documented in Figure 9 and hence, an intensification of cold and saline water advection from the eastern to the western tropical Pacific. This surface transport anomaly in the warm pool area increases the surface density of the warm pool waters, destroying the very stable stratification of the warm pool that is established by a shallow freshwater cap in both present-day and simulated glacial conditions. Salinity maxima and minima in the MW experiment (years 200-500) can be observed at depths of 150-200m and 500-1000m, respectively. In turn, the freshwater cap of the warm pool is mixed with cold and salty waters from below. In addition to the salinity and cold water advection due to an enhanced South Equatorial Current, the vertical mixing contributes to the generation of a positive sea surface salinity anomaly (Figure 9) of about 0.3-0.5 psu and a negative sea surface temperature anomaly of -0.6 K.

5. Summary and Discussion

We studied the response of the global climate system to Heinrich events using a coupled atmosphere-ocean model of intermediate complexity. We presented modeling evidence for a rapid oceanic teleconnection between sea-level variations in the glacial North Atlantic, such as those recorded e.g. during Heinrich events, and sea level variations of opposite phase in the tropical Pacific. When sealevel in the North Atlantic increases due to meltwater injections, a thermocline (see Figure 8) and sea-level gradient is established by baroclinic global ocean adjustment[2] between the ocean basins that drives anomalous geostrophic surface and subsurface current anomalies and enhances the transport of cold waters and salty into the Pacific warm pool area. This effect is furthermore amplified by a tradewind intensification[3] in the Pacific ocean and a reduction of precipitation in the Pacific warm pool, triggered by a change of the global meridional surface temperature gradient during the shutdown phase of the meridional overturning circulation. Furthermore, this gradient leads to a weakening of the summer monsoons over India and Southeast Asia as well as to reduced precipitation over northern South America and an intesification of precipitation over Northern Australia, in accordance with recent paleo-reconstructions. Further evidence supporting our conclusions comes from an analysis of reconstructed Sulu sea surface salinity variations (Rosenthal et al. [2003]) during deglaciation. Sea surface salinity anomalies in this area parallel climate fluctuations in Greenland. In the MD972141 record from the Sulu sea area heavy δ^{18}O values (high salinity) coincide with Heinrich event 1 and the Younger Dryas event (Rosenthal et al. [2003]), whereas low values are found for instance during the Bolling transition. This general pan-oceanic pattern of reconstructed salinity variations during the deglaciation is consistent with the proposed global teleconnection mechanism which involves both the ocean (Figures 8) and the atmosphere (Figure 6).

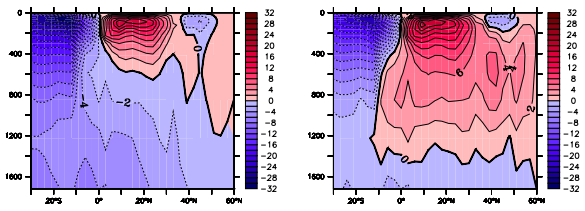

Figure 10. Pan-oceanic overturning seesaw: Left: Meridional streamfunction [Sv] of the Pacific ocean averaged over the first 50 years of the Heinrich simulation. No significant changes of North Atlantic deepwater formation have occured. Right: same as left but averaged for the years 250-300 of the Heinrich simulation. Significant changes in the North Pacific occur as a result of the THC shut-down in the North-Atlantic.

Recently, it was found (Saenko et al. [2004]) that a collapse of the meridional overturning circulation in the North Atlantic may lead to the establishment of an intermediate overturning circulation in the North Pacific with deep water formation in the northern North Pacific. This North Atlantic–North Pacific seesaw effect is also simulated in our MW experiment (see Figure 10). The trigger for the generation of North Pacific Deep Water during Heinrich events is the geostrophic salinity transport induced by the quasi-stationary thermocline field that originates from the global wave adjustment in response to the North Atlantic density anomalies. The salinity increase is further amplified by the Stommel feedback (Stommel [1961]) as proposed by (Saenko et al. [2004]). Hence, the global thermocline adjustment induces a geostrophic salinity transport into the extratropical North Pacific. This transport destabilizes the water column by increased northward surface salinity transport (not shown) thereby generating a North Pacific intermediate overturning cell. In turn, the changed subtropical (southward shift) and supolar gyres (see Figure not shown) induce a weak warming of up to 1.5 K in the eastern North Pacific and a cooling of about -1.5 K in the northwestern Pacific Kuroshio extension region (see Figure 3). The reconstructed warming of about 3-6 K (Kiefer et al. [2001]) is not simulated as a large-scale feature here. In a forthcoming study we will address the question whether a possible future weakening of the thermohaline circulation due to greenhouse warming may have a similar influence on global thermocline patterns (Hsieh and Bryan [1996]), tropical climate and ENSO variability.

Our modeling results suggest the global pattern of millennial-scale climate change can be explained without invoking a link between El Niño and stadials (Stott et al. [2002]), although our study does not exclude this possibility. Previous findings from paleo-reconstructions can be explained in terms of North Atlantic forcing only.

6. Figure captions

Figure 1 Extratropical-tropical connections: Normalized and inverted time series of Δ^{18}O of planktonic formanifera (red) in the Pacific warm pool core MD98-2181 (Stott et al. [2002]). The largest Δ^{18}O variations for Globigerinoides ruber represent local salinity variations and are coherent with the DO cycles, as recorded in the normalized δ^{18}O of

planktonic foraminifera (blue) sampled off the Iberian margin (Shackleton et al. [2000]). Both records are shown on the GISP2 timescale (Blunier and Brook [2001]).

Figure 2 Left: Observed averaged ERA40 2m temperature (http://www.ecmwf.int/research/era/Data_Services/). Right: Simulated averaged 2m temperature for a 280 ppm CTR simulation using ECBilt-Clio.

Figure 3 Reconstructed and simulated glacial sea surface temperature (SST) anomalies: Upper panel: Difference between reconstructed North Atlantic GLAMAP (Sarnthein et al. [2003]) and Pacific and Indian ocean (CLIMAP [1981]) sea surface temperature (time average of February and August) for the Last Glacial Maximum and the present-day SST (CLIMAP [1981]). Middle panel: Sensitivity of the simulated annual mean SST to glacial boundary conditions as quantified by the difference of the equilibrated time-mean SST of the LGM experiment and the pre-industrial CTR experiment. Lower panel: Simulated SST difference between a collapsed THC state during the LGM (time average of years 200-300 in experiment MW) and normal LGM conditions.

Figure 4 North Atlantic-tropical Pacific teleconnections: Simulated time series of the meridional ocean transport across 30^{o}S in the North Atlantic [Sv=10^6 x m^3/s] (blue) and area averaged salinity [psu] in the Pacific warm pool (15^{o}S-15^{o}N, 120^{o}E -160^{o}E) area.

Figure 5 Atmospheric response to Heinrich event: Upper panels: Difference of time averaged wind stress (vectors), temperature (shading) fields of MW and LGM (left) and MW and MW2 (right). The time average is representing the THC shutdown state and is computed form the simulation years 250–300. Lower panels: Same as upper panels but for evaporation minus precipitation [cm/year].

Figure 6

Figure 7 Global sea-level seiching: Left: Basin averaged sea level evolution [m] of the Atlantic, Pacific and Indian ocean basins simulated by the fully coupled meltwater experiment (MW). The sea level anomalies between Atlantic and Pacific exhibit an out-of-phase relationship which is typical for standing waves - so called global sea level seiches. Right: As left but for the global uncoupled experiment (MW1).

Figure 8 Thermocline response to a THC shutdown: Difference of the time-averaged depth of the isopycnal 26.0 kg/m^3 surface between a collapsed THC state (years 200-300 in MW) and an un-collapsed LGM THC state (years 1-30 in MW). The 26.0 kg/m^3 isopycnal surface separates upper-ocean thermocline waters from deep ocean waters. An overall deepening of the North Atlantic thermocline is accompanied by a deepening of the thermocline in the other tropical oceans.

Figure 9 Mechanism for warm pool salinity changes: time-depth diagram of area-averaged salinity [psu] near the core site of MD98-2181 (shaded) and zonal currents (contour, the contour interval is 2 cm/s).

Figure 10 Pan-oceanic overturning seesaw: Left: Meridional streamfunction [Sv] of the Pacific ocean averaged over the first 50 years of the Heinrich simulation. No significant changes of North Atlantic deepwater formation have occured. Right: same as left but averaged for the years 250-300 of the Heinrich simulation. Significant changes in the North Pacific occur as a result of the THC shut-down in the North-Atlantic.

Acknowledgments. U.Krebs, F. Justino and A. Timmermann were supported from the Collaborative Research Project SFB460 of the Deutsche Forschungsgemeinschaft. A. Timmermann has been further supported by the Japan Agency for Marine-Earth Science and Technology (JAMSTEC) through its sponsorship of the International Pacific Research Center. We are grateful to Lowell Stott for his very valuable and constructive comments on an earlier version of the manuscript. We also thank Gisela Speidel for her careful editing of an earlier version of the manuscript.

Notes

1. Note, however, that the exact phase-difference between these curves is uncertain and the apparent correlation between stadials and saline conditions in the warm pool may be an artefact of using the joint GISP2 timescale, assuming already a certain type of wiggle-matching and correlation.
2. A part of the global oceanic standing wave travels through the Indonesian passages as an equatorial viscous boundary wave. Because our LGM model configuration does not take into account the drop of global sea level during glacial times and the glacial topography of the Indonesian passages is not represented precisely. the details of the wave propagation around the maritime continent may have been different furing glacial periods. However, as these waves lead to an overall baroclinic sea level and density adjustment we may assume that under glacial topographic conditions also a strong large-scale connection existed between the Indian and Pacific oceans.
3. The coupled atmosphere-ocean-sea-ice model employed here somewhat underestimates the tropical air-sea coupling (Timmermann et al. [2004]). Hence, the amplitude of the thermocline anomaly pattern (see Figure 8) generated during the THC shutdown phase may be too small, but its qualitative structure appears to be robust.

References

H. Annamalei, P. Liu and S.-P Xie Southwest Indian Ocean SST Variability: Its Local Effect and Remote Influence on Asian Monsoons. *J. Climate*, accepted, 2005.

E. Bard. Comparison of alkenones estimates with other paleotemperature proxies. *Geochemistry, Geophysics, Geosystems*, 2: 1–12, 2001.

T. Blunier and E. Brook. Timing of Millennial-Scale Climate Change in Antarctica and Greenland During the Last Glacial Period. *Science*, 291: 109–112, 2001.

J.M Campin and H. Goosse. A parameterization of dense overflow in large-scale ocean models in z coordinate. *Tellus*, 51A:412–430, 1999.

M. Cane. Climate Change: A Role for the Tropical Pacific. *Science*, 282: 59–61, 1998.

P. Cessi, K. Bryan, and R. Zhang. Global seiching of thermocline waters between the Atlantic and the Indian-Pacific Ocean Basins. *Geophys. Res. Lett.*, 31:doi: 10.1029/2003GL019091, 2004.

CLIMAP. Seasonal reconstruction of the Earth's surface of the last glacial maximum. *Geol. Soc. Am. Map. Chart Ser.*, MC-36, 1981.

T.J. Crowley and S.K. Baum. Effect of vegetation on an ice-age climate model simulation. *J. Geophys. Res.*, 102:16,463–16,480, 1997.

W. Dansgaard, S. J. Johnsen, H. B. Clausen, D. Dahl-Jensen, N. S. Gundestrup, C. U. Hammer, C. S. Hvidberg, J. P. Steffensen, A. E. Sveinbjrnsdottir, J. Jouzel, and G. Bond. Evidence for general instability of

past climate from a 250-kyr ice-core record. *Nature*, 364: 218–220, 1993.

B.W. Dong and R.T. Sutton Adjustment of the coupled ocean-atmosphere system to a sudden change in the Thermohaline Circulation. *Geophys. Res. Lett.*, 29: 10.129/2002GL015229, 2002.

P.R. Gent and J.C. McWilliams. Isopycnal mixing in ocean general circulation models. *J. Phys. Oceanogr.*, 20:150–155, 1990.

A.E. Gill. Some simple solutions for heat induced tropical circulation. *Quart. J. Roy. Meteor. Soc.*, 106:447–462, 1980.

H. Goosse, E. Deleersnijder, T. Fichefet, and M.H. England. Sensitivity of a global coupled ocean-sea ice model to the parameterization of vertical mixing. *J. Geophys. Res.*, 104(C6):13681–13695, 1999.

H. Goosse and T. Fichefet. Importance of ice-ocean interactions for the global ocean circulation: a model study. *J. Geophys. Res.*, 104(C10):23337–23355, 1999.

H. Heinrich. Origin and consequences of cyclic ice rafting in the Northeast Atlantic-Ocean during the past 130,000 years . *Quat. Res.*, 29: 143–152, 1988.

I.M. Held and M.J. Suarez. A two-level primitive equation atmosphere model designed for climate sensitivity experiments. *J. Atmos. Sci.*, 35:206–229, 1978.

S.W. Hostetler and A.C. Mix. Reassessment of ice-age cooling of the tropical ocean and atmosphere. *Nature*, 399:673–676, 1999.

W. W. Hsieh and K. Bryan. Redistribution of sea level rise associated with enhanced greenhouse warming: a simple model study. *Climate Dynamics*, 12:535–544, 1996.

W.M. Hsieh, M. K. Davey, and R.C. Wajsowicz. The free Kelvin wave in finite-difference numerical models. *J. Phys. Oceanogr.*, 13:1381–1397, 1983.

R.X. Huang, M.A. Cane, N. Naik, and P. Goodman. Global adjustment of the thermocline in response to deepwater formation. *Geophys. Res. Lett.*, 27:759–762, 2000.

T.S. Ivanochko, R.S. Ganeshram, G.-J.A. Brummer, G. Ganssen, S.J.A. Jung, S.G. Moreton, and D. Kroon. Variations in Tropical Convection as an Amplifier of Global Climate Change at the Millennial Scale. *Earth. Planet. Sci. Lett.*., submitted , 2005.

H. Johnson and D.P. Marshall. A Theory for the Surface Atlantic Response to Thermohaline Variability. *J. Phys. Oceanography*, 32: 1121–1132, 2002.

M. Kawase. Establishment of deep ocean circulation driven by deep-water production. *J. Phys. Oceanogr.*, 17:2294–2317, 1987.

L.D. Keigwin and S. J. Lehman. Deep circulation change linked to Heinrich Event 1 and Younger Dryas in a mid-depth North Atlantic core. *Paleoceanography*, 9: 185–194, 1994.

T. Kiefer, M. Sarnthein, P.M. Grootes, and A.P. Roberts. North Pacific response to millennial-scale changes in ocean circulation over the last 60ky. *Paleoceanography*, 16:179–189, 2001.

A. Kitoh, S. Muakami, and H. Koide. A simulation of the Last Glacial Maximum with a coupled atmosphere-ocean GCM. *Geophys. Res. Lett.*, 28:2221–2224, 2001.

R. Knutti, J. Flückiger, T. Stocker, and A. Timmermann. Strong hemispheric coupling of glacial climate through freshwater discharge and ocean circulation. . *Nature*, 430: 851-856, 2004.

A. Koutavas, J. Lynch-Stieglitz, Jr. T.M. Marchitto, and J.P Sachs. El Niño-like Pattern in Ice Age Tropical Pacific Sea Surface Temperature. *Science*, 297:226–230, 2002.

C. Lang, M. Leuenberger, J. Schwander, and S. Johnsen. 16^0C Rapid Temperature Variation in Central Greenland 70,000 Years Ago. *Science*, 286:934–937, 1999.

D.W. Lea, D. K. Pak, and H. J. Spero. Climate impact of late quaternary equatorial pacific sea surface temperature variations. *Science*, 289:1719–1724, 2000.

R.E. Livezey, M. Masutani, A. Leetmaa, H. Rui, M. Ji, and A. Kumar. eleconnective response of the Pacific-North American region atmosphere to large central equatorial Pacific SST anomalies. *J. Climate*, 10:1787–1820, 1997.

M. Lyle, F. Prahl, and M. Sparrow. Upwelling and productivity changes inferred from a temperature record in the equatorial Pacific . *Nature*, 355:812–815, 1992.

J. Marshall and F. Molteni. Toward a dynamic understanding of planetary-scale flow regimes. *J. Atmospheric Sciences*, 50:1792–1818, 1993.

G.L. Mellor and T. Yamada. Development of a turbulence closure model for geophysical fluid problems. *Rev. Geophys. Space Phys.*, 20:851–875, 1982.

J.D. Opsteegh, R.J. Haarsma, F.M. Selten, and A. Kattenberg. ECBILT: A dynamic alternative to mixed boundary conditions in ocean models. *Tellus*, 50A:348–367, 1998.

W.R. Peltier. Ice age paleotopography. *Science*, 265:195–201, 1994.

L.C. Peterson, G.H. Haug, K.A. Hughen, and U. Rohl. Rapid changes in the hydrologic cycle of the tropical Atlantic during the last glacial. *Science*, 290:1947–1951, 2000.

S. Rahmstorf. Timimg of abrupt climate change: a precise clock. *Geophys. Res. Lett.*, 30, 2003.

D. Roche, D. Paillard, and E. Cortijo. Constraints on the duration and freshwater release of Heinrich event 4 through isotope modeling. *Nature.*, 432, 379–382, 2003.

Y. Rosenthal, D. W. Oppo, and B. K. Linsley. The amplitude and phasing of climate change during the last deglaciation in the Sulu Sea, western equatorial Pacific. *Geophys. Res. Lett.*, 30:1428 doi: 10.1029/2002GL016612, 2003.

Saenko, A. Schmittner, and A. Weaver. The Atlantic-Pacific Seesaw. *J. Climate*, 17:2033–2038, 2004.

M. Sarnthein, U. Pflaumann, and M. Weinelt. Past extent of sea ice in the northern North Atlantic inferred from foraminiferal paleotemperature estimates. *Paleoceanography*, 18:1047, doi:10.1029/2002PA000771, 2003.

H. Schultz, H . Erlenkeuser and U. von Rad. Correlation between Arabian Sea and Greenland climate oscillations of the past 110,000 years. *Nature*, 393:54–57, 1998.

J.P. Severinghaus and E.J. Brook. Abrupt Climate Change at the End of the Last Glacial Period Inferred from Trapped Air in Polar Ice. *Science*, 286:930–934, 1999.

N.J. Shackleton, M.A. Hall, and E. Vincent. Phase relationships between millennial scale events 64000 to 24000 years ago. *Paleoceanography*, 15:565-569, 2000.

M. Sidall, E. J. Rohling, A. Almogi-Labin CH. Hemleben, D. Meischners, I. Schmelzer, and D. A. Smeed. Sea-level fluctuations during the last glacial cycle. *Nature*, 423:853–858, 2003.

T. F. Stocker and S.J. Johnsen. A minimum thermodynamic model for the bipolar seesaw. *Paleoceanography*, 18:1087, doi:10.1029/2003PA000920, 2003.

H.M. Stommel. Thermohaline convection with two stable regimes of flow. *Tellus*, 13:224–230, 1961.

L. Stott, C. Poulsen, S. Lund, and R. Thuell. Super ENSO and Global Climate Oscillations at Millennial Time Scales. *Science*, 297:222-226, 2002.

A. Timmermann, F. Justino, F.-F. Jin, U. Krebs, and H. Goosse. Surface temperature control in the North and tropical Pacific during the last glacial maximum. *Climate Dyn.*, 23:353–370, 2004.

A. Timmermann, M. Schulz, H. Gildor, and E. Tziperman. Coherent resonant millennial-scale climate oscillations triggered by massive meltwater pulses. *J. Climate*, 16:2569-2585, 2003.

C.S. Turney, A.P. Kershaw, S.C. Clemens, N. Branch, P.T. Moss, and K. Fifield. Synchronous Millennial-Scale Climatic Oscillations of the tropical Pacific and north Atlantic Oceans . *Nature*, 428:306–309, 2004.

M. Watanabe, F.-F. Jin. A moist linear baroclinic model: Coupled dynamical-convective response to El Niño . *J. Climate*, 16:1121-1139, 2003.

Y. Yokoyama, T.M. Esat, and K. Lambeck. Coupled climate and sea-level changes deduced from Huan Peninsula coral terraces of the last ice age. *Earth Plan. Sci. Lett.*, 193: 579–587, 2001.

A. Timmermann, International Pacific Research Center, SOEST, University of Hawai'i, 1680 East-West Road, Honolulu, HI 96822, USA (axel@hawaii.edu)